Fuel cells: Materials needs and advances

Zongping Shao* and Meng Ni

Fuel cells are highly efficient electrochemical energy-conversion devices with a wide application potential, spanning from portable power sources to stationary power generation. They are typically categorized according to their operating temperature, for example, low temperature (<100°C), intermediate temperature (450–800°C) and high temperature (>800°C). Recently, reduced temperature fuel cells operating at 200–400°C have also received considerable attention for their multiple benefits. A single fuel cell is composed of a porous anode for fuel oxidation, a dense electrolyte for ion transportation, and a porous cathode for oxygen reduction. Due to their different functions and operating environments, each layer of the cell faces unique materials requirements in terms of ionic and electronic conductivity, chemical and mechanical stability, thermal expansion, etc. This article gives a thorough perspective on the challenges and recent advances in anode, electrolyte, and cathode materials for the various types of fuel cells. Emerging fuel cells operating at 200–400°C are also discussed and commented. Finally, the key areas of need and major opportunities for further research in the field are outlined.

Introduction

The extensive use of nonrenewable fossil fuels based on low-efficient combustion has brought serious concerns about air pollution, water pollution, and climate change. Eighty-nine percent of global CO_2 emissions were found to come from fossil fuels and industry in 2018.[1] To realize a sustainable development of our society, it is well agreed that we need to build a new carbon-neutral energy system, which calls urgently for innovative carbon-zero energy materials and advanced energy utilization technologies.

Fuel cells are electrochemical energy-conversion devices that directly transform the chemical energy stored in a fuel into electric power by avoiding Carnot cycle limits, showing advantageous features of high efficiency and low emissions. Although the first fuel cell was demonstrated more than a century ago,[2] they are receiving increased research attention today as the world moves toward a net-zero CO_2 emission society. Fuel cells not only offer high energy efficiency and low emissions, but also present additional advantages, such as high energy density, size flexibility, salient operation, and reliability.[3] Potential application fields range from power sources for small portable devices to large stationary power generation.

A complete, integrated fuel-cell system is composed of one or more cell stacks in addition to gas delivery, thermal management, and electrical control components. A fuel-cell stack is composed of multiple individual fuel cells connected together in series. Each cell consists of a porous cathode and a porous anode with a dense electrolyte sandwiched between them. The cathode hosts the oxygen reduction reaction (ORR), while fuel oxidation occurs at the anode. The electrodes need to be porous, catalytically active, and ionic and electronically conductive to accommodate gas flow while facilitating electrochemical reactions, whereas the electrolyte must be dense and pinhole-free to prevent fuel-oxidant mixing and provide high ionic conduction while inhibiting electronic leakage.

Different types of fuel cells often have distinctly different applications. In addition to categorization by operating temperature,[4] they can also be categorized by the ionic conduction mechanism of the electrolyte,[5] or the intended fuel.[6] The most common fuel-cell electrolyte types include those that can conduct oxygen ions—as in solid-oxide fuel cells (SOFCs),[7,8] protons—as in Nafion-based polymer electrolyte membrane fuel cells (PEMFCs),[9,10] protonic ceramic fuel cells (PCFCs),[11,12] or solid acid fuel cells (SAFCs),[13] CO_3^{2-} for molten carbonate fuel cells (MCFCs),[14] or OH^- as in anion exchange membrane fuel cells (AEMFCs),[15] or molten alkaline fuel cells (MAFCs).[16] Considering potential

Zongping Shao, WA School of Mines: Minerals, Energy and Chemical Engineering (WASM-MECE), Curtin University, Perth, WA, Australia; zongping.shao@curtin.edu.au
Meng Ni, Department of Building and Real Estate, Research Institute for Sustainable Urban Development (RISUD) & Research Institute for Smart Energy (RISE), The Hong Kong Polytechnic University, Hong Kong, China; meng.ni@polyu.edu.hk
*Corresponding author
doi:10.1557/s43577-024-00722-9

operating temperature ranges, low-temperature fuel cells (<100°C) are more promising for portable or mobile application, but typically require precious metal catalysts for sufficient electrochemical performance, which are costly and highly sensitive to gas poisoning. Intermediate (450−700°C) and high-temperature fuel cells (>700°C) facilitate faster electrode reaction kinetics and increased options for ionic transport, thus greatly broadening the materials selection. However, sealing and thermal management concerns become significant.[17] Among the different types of fuel cells, PEMFCs and SOFCs have received the most attention due to their adequate level of maturity and many benefits as compared to the other types of fuel cells. For PEMFCs, there is a drive to increase their operation temperature to enhance the electrode reaction kinetics, whereas for SOFCs there are intensive efforts to reduce operation temperature from conventionally higher than 800°C to the intermediate range of 450−700°C or even to the lower range of 200–400°C.

General materials requirements for key fuel-cell components

Electrolyte

The electrolyte plays two key roles in a fuel cell (i.e., it physically separates the fuel and oxidant (air or oxygen) gases, and it conducts ion while blocking electron). Therefore, fuel-cell electrolytes should be dense and show pure ionic conductivity. However, some electrolyte membranes are nevertheless semipermeable to certain reactants. For example, the (undesirable) crossover of methanol is observed in Nafion-based membranes.[18] During operation, this diffusion of methanol from anode to cathode results in a mixed potential at the cathode and reduces faradic efficiency in Nafion-based direct methanol fuel cells (DMFCs).

Regardless of whether the ionic conducting species is H^+, O^{2-}, CO_3^{2-}, OH^- and even H_3O^+, an ionic conductivity of 1×10^{-2} S cm^{-1} or higher for the electrolyte is preferred at the target operating temperature to ensure the favorable cell performance.[19] Since the anode experiences a reducing atmosphere while the cathode atmosphere is oxidizing, the electrolyte should show stable phase structure and chemical stability and maintain pure ionic conductivity over a wide range of oxygen partial pressure. In doped ceria, a common SOFC electrolyte, thermal reduction of Ce^{4+} to Ce^{3+} occurs above 650°C, introducing partial electronic conductivity into the electrolyte; therefore, doped ceria is applicable only for operating temperatures <650°C.[20] Another example is Bi_2O_3 and various doped "BIMEVOX"-based electrolytes. Although conductivities >0.94 S cm^{-1} at 650°C are reported,[21,22] their instability in reducing atmosphere limits their application in fuel cells. Electrolyte membranes are also required to show sufficient mechanical strength, especially in electrolyte supported cells.[23] The chemical and thermomechanical compatibility of the electrolyte with other cell components is also critical, especially for ceramic-based elevated temperature fuel cells.[24,25] Although some reported materials show promisingly high conductivity, their easy reaction with electrode materials challenges their practical use in fuel cells.[26,27] Up to now, practically applicable electrolyte materials remain quite limited, as the development of new electrolyte materials must take into account all the previously mentioned factors.

Cathode

The electrochemical ORR proceeds at distinct active sites known as triple-phase boundaries (TPB) in the cathode, which are formed by the simultaneous convergence of the catalyst, electrolyte, and gas (pore) phases. An ideal cathode should exhibit a high density of TPBs with high ORR activity and durability at the target operating temperature. If the cathode also possesses ionic conductivity of similar magnitude to the electrolyte, the reaction can extend to the catalyst-gas "dual-phase boundaries." Thus, introducing ionic conductivity into the cathode material is highly valued, and can be achieved by materials design of single-phase mixed ionic–electronic conducting (MIEC) electrodes,[28] or by introducing an ionic conducting second phase.[29] For PCFCs, oxygen ion, proton, and electron-conducting "triple conductors" are even preferred. The conductivity of the individual species should be well tailored to maximize the electrode performance. Because the cathode operates in an oxidizing atmosphere, it should also show sufficient antioxidizing capability. High electronic conductivity is also needed. Carbon-based materials are desirable cathodes in low-temperature fuel cells due to their high electronic conductivity; however, some activated carbon-based electrocatalysts demonstrate insufficient stability in elevated temperature fuel cells, including PCFCs and SOFCs, where oxide-based electrodes are adopted instead. Perovskite oxides extensively used as cathodes in SOFCs like $La_{0.8}Sr_{0.2}Co_{0.6}Fe_{0.4}O_{3-\delta}$ (LSCF) and $La_{0.8}Sr_{0.2}MnO_{3-\delta}$ (LSM) show high electronic conductivity (~1000 S cm^{-1}).[30,31] Chemical stability against impurities in air or reaction products is also a big concern. For example, the minor amount of CO_2 in air could react with perovskite-type SOFC cathodes with the formation of surface carbonate or even bulk carbonate, causing a quick decay in performance.[32,33] In PCFCs, water is formed at the cathode. High concentrations of water vapor could cause the collapse of perovskite structure. Thus, the phase stability of PCFC cathodes against both CO_2 and H_2O is of concern.[34,35] In addition, chemical and thermomechanical compatibility of the cathode with other cell components should also be considered, especially for ceramic fuel cells operating at elevated temperatures. Phase reactions could form an insulating interfacial layer between the cathode and electrolyte, thus significantly increase the ohmic resistance of the cell,[36] while a mismatch in thermal expansion behavior between cathode and electrolyte could cause electrode delamination,[37] especially during thermal cycling, leading to a quick cell performance decay, or even failure.

Anode

The anode performs electrochemical fuel oxidation. Similar to cathodes, anodes should possess high electrocatalytic activity and electronic conductivity to ensure low activation polarization and ohmic polarization resistance. Mixed ionic and electronic conductivity is also favorable for anodes. The chemical and thermomechanical compatibility with other cell components, in particular with the electrolyte, is also crucial. Because the anode operates in a reducing atmosphere, low-temperature fuel cells typically employ carbon-based substrates,[38] while metallic nickel is often applied as the electron-conducting phase and electrocatalyst for elevated temperature fuel cells.[39] To minimize interfacial resistance and to improve thermomechanical compatibility, the electrolyte phase is typically introduced into the anode to form a composite electrode. The required anode catalyst loading is typically lower than for the cathode due to the lower overpotential for fuel oxidation, but anode catalysts require anti-poisoning capability to deal with some impurities in fuels. Because hydrogen produced from reforming gas could contain CO, CO poisoning is a concern in low-temperature fuel cells and can lead to significant degradation of cell performance,[40] while the coking resistance is crucial in the development of elevated temperature ceramic fuel cells for operation with hydrocarbon fuels. Some fuel cells enable power and chemicals cogeneration. Under this circumstance, the anode should possess high selectivity toward the targeted product during operation, which places additional requirements on anode development. With increased fuel conversion, the oxygen partial pressure at the anode can increase substantially, which could lead to anode oxidation. Repeated redox of the anode materials could cause electrode pulverization. Thus, the redox stability also needs to be examined in anode development, especially for ceramic fuel cells.

Advances in fuel-cell materials

Low-temperature polymer-exchange membrane fuel cells

Low-temperature polymer-exchange membranes mainly include proton exchange membranes (PEMs) and anion exchange membranes (AEMs). PEMs operate under acidic conditions, exchanging protons from the anode to the cathode, whereas AEMs operate under alkaline conditions, transferring hydroxide ions from the cathode to the anode. PEMFCs have achieved a certain level of commercial maturity. Cost and durability are the key factors for commercialization. Most PEMFCs employ perfluorosulfonic acid (PFSA)-based membranes (such as Nafion) as they feature high proton conductivity (~100 mS cm^{-1}) at room temperature and good chemical and mechanical stability. To increase performance, the field has moved toward ever thinner electrolyte membranes that reduce ohmic losses by shortening the proton and water transport path and also mitigate dehydration. Membranes as thin as 8−10 μm have recently been adopted in commercial PEMFC stacks.[41] Researchers are also working to improve chemical, mechanical, and thermal stability. To adapt to specific applications, such as dry conditions, higher operating temperatures, and/or tolerance to liquid methanol for DMFCs, composite membranes have been developed by modifying PFSA membranes with various inorganic materials, metal oxides,[42–44] metal phosphates,[45] zeolites,[46] or graphene oxides.[47] Although these modifications generally lead to reduced proton conductivity, they bring benefits like enhanced mechanical strength and improved water retention capacity for operating under low gas humification, improved durability for operating at temperatures >100°C, as well as the ability to inhibit methanol crossover. Metal–organic frameworks (MOFs) have also been used in polymer composite membranes; such composites often exhibit outstanding proton conductivity and good stability, and thus offer significant promise.[48,49] In these composites, co-percolation of the two phases enables continuous and sufficient proton conduction along the MOF/polymer matrix interfaces.

Platinum carbon (Pt/C) is standard catalyst in PEMFCs for both the hydrogen oxidation reaction (HOR) and ORR. A high Pt loading of 50−60% on carbon is preferably used to build a thinner catalyst layer to benefit mass transport and water management. To reduce Pt loading and decrease costs, Pt-alloy catalysts, such as Pt–Co and Pt–Ni, with special morphological structures are particularly valued. Recently, larger-sized catalyst particles (~15 nm) with a nanoporous substructure have been demonstrated to exhibit improved H_2-air fuel-cell performance versus smaller 5-nm solid core–shell nanoparticles, which also featured high specific surface area (**Figure 1**).[15] The improvement was attributed to enhanced O_2 diffusion and efficient H^+ surface conduction on Pt enabled by the nanoporous architecture, which underscores the role of maximizing the mass activity of Pt for high-power-density fuel-cell applications.

AEMFCs have attracted tremendous recent interest as the alkaline condition enables the use of lower-cost precious-metal-free electrocatalysts.[50] AEMs generally consist of a hydrophobic polymer backbone functionalized with positive cations, typically quaternary ammonium ($–NR^{3+}$) groups. The OH^- anions are conducted based on the interactions between the hydrophilic, positively charged functional groups and the negatively charged OH^-. As an emerging field, new AEMs are being developed at a greater pace than new PEMs, and the reported ionic conductivity of AEMs under humification is approaching that of PEMs.[51] Some radiation-grafted AEMs show conductivities >200 mS cm^{-1}, and have been used to achieve competitive AEMFC performance of 2.0 W cm^{-2} (albeit under H_2/O_2, with a PtRu/C anode and a Pt/C cathode).[52] Several functional groups besides $–NR^{3+}$ have been explored, including pyridinium, imidazolium, pyrrolidinium, phosphonium, benzimidazolium, etc., to improve stability.[53] Despite groundbreaking progress, the electron-deficient cationic functional groups appended to the polymer backbone for OH^- conduction are very susceptible to hydroxide attack, thus the long-term stability of AEMs is still a significant issue. Currently, reported AEMs are generally tolerant to operating

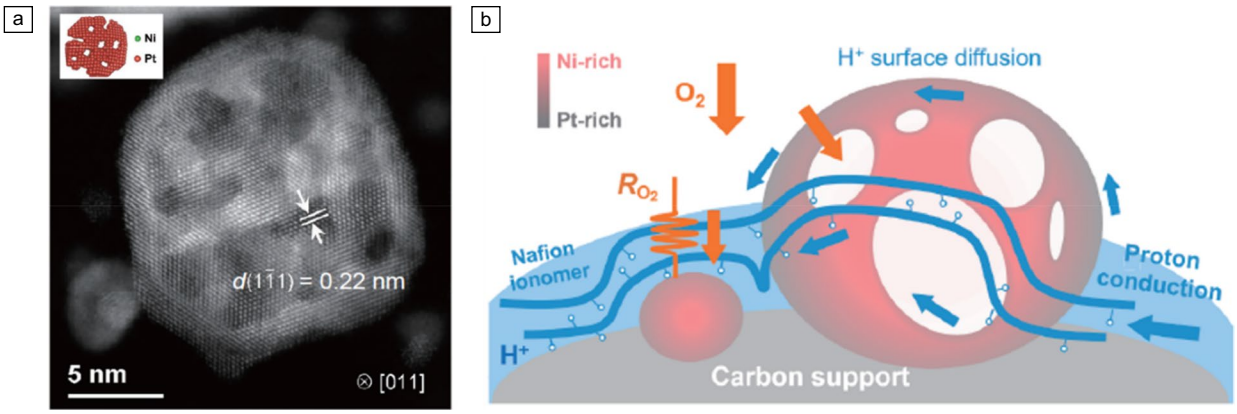

Figure 1. (a) High-resolution transmission electron microscopy image of the $PtNi_3$/C-600 catalyst with nanoporous structures. (b) Schematic illustration of the interactions of the large nanoporous particle and the small solid particle with ionomer in catalyst layer, and the mass transportation involved in the electrochemical reaction.[15]

temperatures <80°C; further increase in temperature typically accelerates the degradation kinetics of the membrane.[54] However, increasing AEMFC operating temperature is desired as it can bring additional benefits to the cell performance by enhancing the electrode reaction kinetics, as well as improving the membrane and cathode hydration status via promoted water diffusion.[55,56]

The alkaline environment enables great flexibility for catalyst design, especially for the ORR at the cathode. Various types of cathode materials, including metal-nitrogen-carbon (M–N–C) catalysts,[57] and transitional-metal oxides have been reported to attain the benchmark AEMFC peak power density threshold of 1 W cm^{-2}.[58] **Figure 2** shows promising platinum-group-metal (PGM)-free cathodes with Fe–N–C,[59] and nitrogen-doped carbon-CoO_x (N–C–CoO_x) nanohybrids[60] that were able to deliver ultrahigh power density exceeding 1 W cm^{-2} under H_2/O_2 reacting gases when paired with a PtRu/C anode. For AEMFCs, the development of PGM-free anodes remains difficult,[61] as the HOR activity in alkaline medium decreases by around two orders of magnitude on common

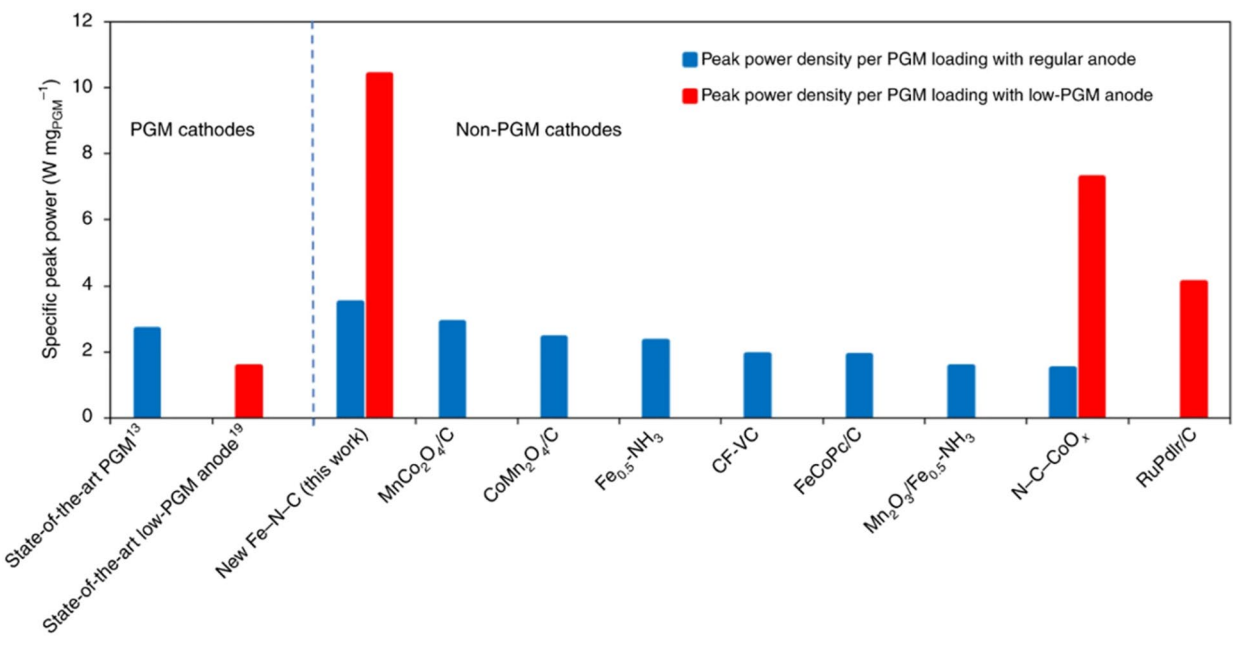

Figure 2. A comparison of the specific peak power (W mg_{PGM}^{-1} loading) of anion exchange membrane fuel cells tested under H_2/O_2 conditions employing platinum-group-metal (PGM)-free electrodes versus state-of-the-art PGM electrodes.[59]

noble metals.[62] Therefore, creating different environments for the anode and the cathode is considered an interesting future direction to optimize cell performance.

High-temperature ceramic fuel cells

SOFC electrolytes should exhibit good ionic conductivity and a compatible coefficient of thermal expansion.[63,64] Oxygen ion-conducting electrolytes, including ZrO_2, CeO_2, LaO_2, and their derivatives are applicable in SOFCs. However, creating electrolytes that are stable at lower temperatures while retaining sufficient ionic conductivity is a significant challenge.[65] Yttria-stabilized zirconia (YSZ), a classical oxygen-ion conductor with excellent ionic conductivity and structural stability at temperatures exceeding 800°C, is largely inadequate at temperatures <650°C.[66–68] Even though scandium-stabilized zirconia (ScSZ) enables further enhancements in conductivity and compatibility, the reactivity of the zirconium-based electrolyte with the cathode can cause cell failure.[69,70] Bismuth oxide (Bi_2O_3), characterized by various phase structures, offers high ionic conductivity in its fluorite structure at elevated temperatures. As the temperature decreases, however, Bi_2O_3 transforms from a fluorite structure to a monoclinic structure, and its ionic conductivity rapidly decreases.[71] In order to stabilize the fluorite phase structure, Verkerk et al.[71] doped Bi_2O_3 with Er (ESB), achieving an ionic conductivity of 0.32 S cm^{-1} at 700°C.[72,73] Introducing a cerium-based oxide layer between the cathode and electrolyte has proven effective in mitigating adverse reactions, attributed to its commendable oxygen-ion conductivity. Further enhancements can be realized through Gd and Sm doping to amplify the ionic conductivity of CeO_2.[74] However, Gd-doped CeO_2 (GDC) and Sm-doped CeO_2 (SDC) exhibit higher electronic conductivity in reducing atmospheres and thus generally cannot be used on their own.[75] $LaGaO_3$-based perovskite electrolytes, notably $La_{0.8}Sr_{0.2}Ga_{0.8}Mg_{0.2}O_{3-\delta}$ (LSGM), have excellent ionic conductivity.[76] However, these materials easily react with Zr-based and Ni-based anodes, which limits their application.

In high-temperature ceramic fuel cells, the cathode requires high oxygen-ion conductivity to maximize ORR activity, but also chemical stability for long-term operation. In a bid to achieve higher electrochemical activity, ion doping, defect modulation, and surface modification are commonly used approaches.[77] Sr deficiency was reported as an effective strategy to enhance the ORR activity and chromium tolerance using entropy-stabilized $Sr_{1-x}Co_{0.5}Fe_{0.2}Ti_{0.1}Ta_{0.1}Nb_{0.1}O_{3-\delta}$ (S_{1-x}CFTTN, x = 0~0.15) cathodes.[78] The Sr-deficient surface suppressed the formation of SrO and $SrCrO_4$ on the cathode (**Figure 3**a). Zhuang et al. achieved the activation of surface Sr atoms by co-sintering MoO_3 with cathode material (($La_{0.6}Sr_{0.4}$)$_{0.95}Co_{0.2}Fe_{0.8}O_{3-\delta}$, LSCF) at high temperature, introducing additional Sr/O vacancies on the surface of LSCF (Figure 3b–c).[79] Chen et al. reported a significant enhancement of

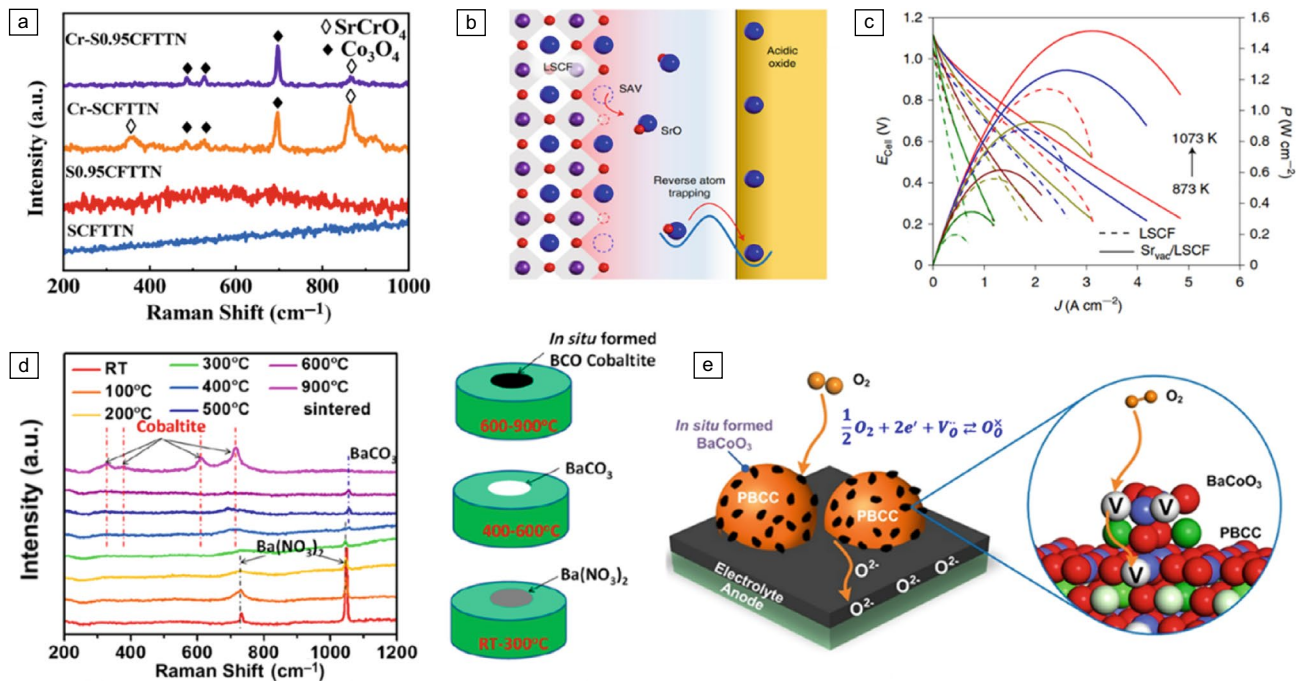

Figure 3. (a) Raman spectra of $SrCrO_4$ and Co_3O_4 on Cr-SCFTTN and Cr-$S_{0.95}$CFTTN cathodes.[78] (b) Schematic illustration of reverse atom trapping.[79] (c) Current–voltage polarization curves and corresponding power densities of the solid-oxide fuel cells with LSCF and Sr_{vac}/LSCF cathodes. (d) *In situ* Raman spectra of PBCC pellet with nanoparticles from room temperature (RT) to 600°C and 900°C. (e) Schematic of electrode reaction processes by forming *in situ* nanostructured $BaCoO_3$ on PBCC.[80] SAV, single atom vacancies.

both the ORR activity and durability by surface modification using a barium nitrate precursor. *In situ* characterization and DFT simulations reveal that the active sites for ORR are primarily in the form of nanoscale particles of barium cobaltite, which are formed above 565°C during the cell startup process (Figure 3d–e).[80]

One of the advantages of SOFCs is the favorable reaction kinetics for fuel reforming or oxidation owing to their wide temperature range (350–800°C). Traditionally, nickel-based ceramics or cermets (ceramic–metal composites) such as Ni-yttria-stabilized zirconia (Ni-YSZ), Ni-Sm-doped CeO_2 (Ni-SDC), Ni-Gd-doped CeO_2 (Ni-GDC), and Ni-$BaCeO_3$-based perovskites are used as anodes due to excellent hydrogen oxidation kinetics, cost-effectiveness, and favorable electronic conductivity, but their stability is challenged due to rapid carbon deposition and sulfur poisoning during fuel oxidation. Unique structured core–shell Ni@GDC[81–83] and novel materials such as $Ce_{0.95}Ru_{0.05}O_{2-\delta}$ (CR5O) have been developed with exceptional fuel flexibility.[84] Although Ni-based cermet anodes exhibit commendable activity and conductivity, they often suffer from Ni agglomeration, structural deterioration, and carbon deposition during operation. Perovskite oxides such as chromites, vanadates, and titanates demonstrate superior resistance to coking, redox stability, and improved electronic and ionic conductivities.[85] However, they generally exhibit lower activity, diminished electrical conductivity, require intricate fabrication processes, and can be thermomechanically incompatibile with the other cell materials. Co–Fe alloy decorated perovskite oxides, such as Ni-doped $La_{0.6}Sr_{0.4}Fe_{0.8}Co_{0.2}O_{3-\delta}$ perovskites,[86] and $Sr_2Fe_{1.4}Co_{0.1}Mo_{0.5}O_{6-\delta}$[87] were developed to operate with various fuels. If carbon-containing fuels are supplied, carbon could cover the TPBs and hinder fuel oxidation. Metallic alloy catalysts with ceria or ruthenium have been reported to effectively suppress coking. Somacescu et al. introduced a bimodal mesoporous $NiO/CeO_{2-\delta}$-YSZ anode for methane oxidation, enhancing the oxygen vacancy content and thereby facilitating carbon removal.[88] To prevent H_2S poisoning, Song et al. reported a novel anode incorporating Ni nanoparticles, $BaZr_{0.4}Ce_{0.4}Y_{0.2}O_{3-\delta}$ perovskite, and amorphous BaO on a $Sm_{0.2}Ce_{0.8}O_{1.9}$ scaffold, which demonstrated superior sulfur tolerance for 50-h operation.[89]

Intermediate-temperature ceramic fuel cells

Lowering the temperature of SOFCs can reduce costs and improve scalability. Recently, several advanced oxygen-ion-based electrolytes have demonstrated good conductivity and performance in the medium temperature range. For example, Xiang et al. developed an SDC@Al_2O_3 core–shell structure composite electrolyte by wrapping a thin layer of amorphous Al_2O_3 around the surface of SDC,[90] which has an ultrahigh ionic conductivity of 0.096 S cm^{-1} (**Figure 4**a). The single cell with this electrolyte achieved a performance of 1190 mW cm^{-2}

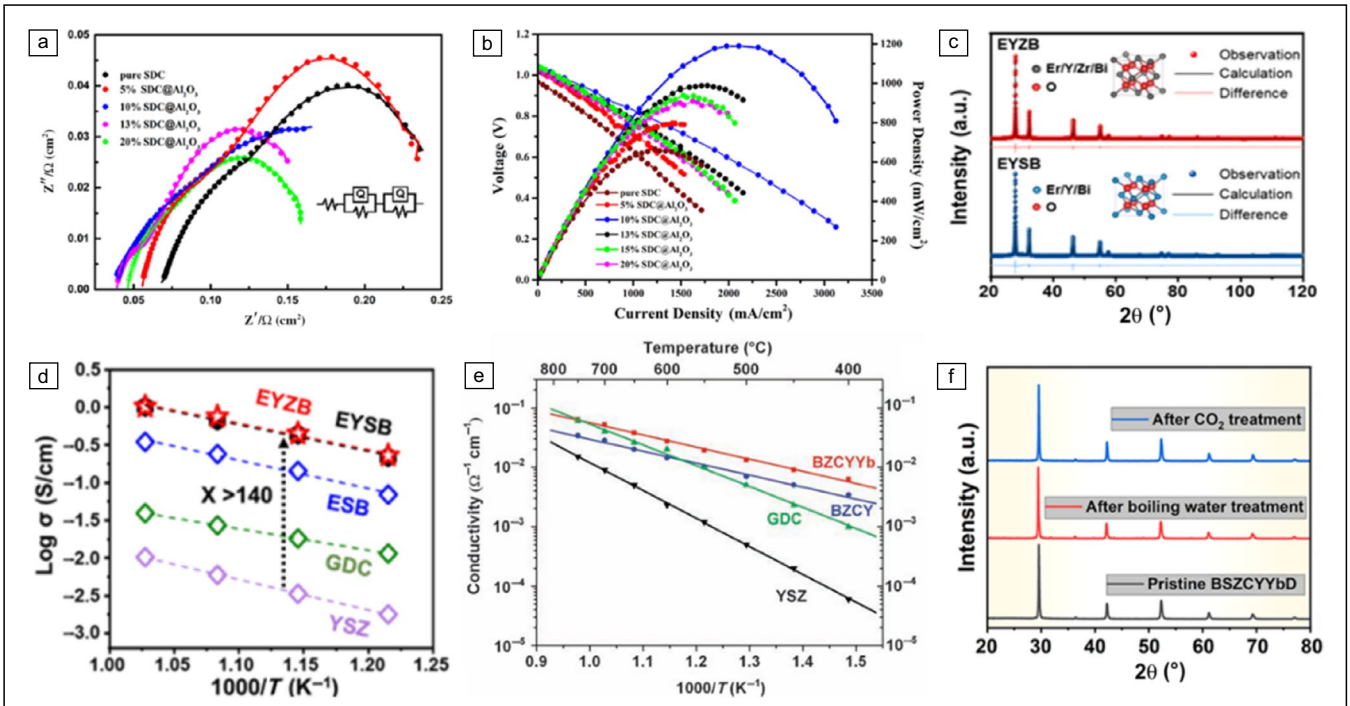

Figure 4. (a) Electrical impedance spectra for the SDC@Al_2O_3 fuel cells, tested in H_2/air atmosphere at 550°C. (b) *I–V* and *I–P* characteristics for the SDC@Al_2O_3 cells. (c) Refined x-ray diffraction (XRD) patterns of EYZB and EYSB.[90] (d) Comparison of electrical conductivities of various oxygen-ion conductors. (e) Ionic conductivities of BZCYYb, BZCY, GDC, and YSZ as measured at 400–750°C in wet oxygen. (f) XRD patterns of BSZCYYbD sample after exposure to a 50% CO_2 atmosphere at 600°C for 10 h and boiling distilled water for 4 h.[91]

at 550°C (Figure 4b). Yu et al. developed a high-performance low-temperature SOFC by doping bismuth oxide with erbium, yttrium, and zirconium (EYZB) (Figure 4c).[91] The ionic conductivity of EYZB at 600°C is 147× higher than that of YSZ (Figure 4d).

PCFCs, as an offshoot of SOFCs, enable lower operating temperatures by employing proton-conducting oxides instead of conventional oxygen-ion-conducting electrolytes. Most PCFCs employ Ba-based perovskite electrolytes ($BaZrO_{3-\delta}$ and $BaCeO_{3-\delta}$), which exhibit a trade-off between conductivity and stability. B-site cation doping emerges as an effective strategy to mitigate this trade-off by introducing multiple elements. Trivalent ions, particularly Y^{3+} and Yb^{3+}, are proved advantageous in B-site doping. Y^{3+}, characterized with a moderate ion radius and a high doping limit, introduces substantial oxygen vacancies, thereby enhancing proton conduction.[92] On the other hand, Yb^{3+} plays a stabilizing role, allowing for a lower Zr content (Figure 4e).[93–95] Certain unique characteristics of specific lanthanide dopants warrant further investigation, such as significantly enhanced sinterability (Pr^{3+}) or chemical stability against CO_2 (Dy^{3+}) (Figure 4f).[96,97] Meanwhile, numerous derivatives have been introduced to improve sintering properties and address conductivity and stability issues.

The development of highly active cathodes at intermediate temperatures has advanced significantly in recent years. Ion doping plays a key role as a simple and effective strategy for improving cathode ion conductivity and catalytic activity.[98,99] Lu et al. utilized codoping with Nb^{5+} and Sc^{3+} to develop a cathode for PCFCs. It was verified that the $BaCo_{0.4}Fe_{0.4}Nb_{0.1}Sc_{0.1}O_{3-\delta}$ (BCFNS) cathode significantly enhanced the hydration capacity and reduced the proton migration barrier due to the synergistic effect between the two ions.[100] Anion and heteroatom doping, such as fluoride (F), boron (B), phosphorus (P), and nitrogen (N) can also modify the activity and structural stability of the cathode.[101,102] Infiltration is often used to decorate the cathode with active or stabilizing second phase nanoparticles. For example, Duan et al. effectively improved ORR catalytic activity by infiltrating BCFZY into a $BaCe_{0.6}Zr_{0.3}Y_{0.1}O_{3-\delta}$ cathode skeleton (**Figure 5**a–b).[103] Second phases can also be generated by *in situ* self-assembly, producing unexpected activity and durability. Proton diffusion and oxygen activation are facilitated by the unique ion-transport and hydration properties of the formed second phase, accelerating the surface reaction kinetics at the cathode. Surface reconstruction is also an effective strategy for constructing composite cathodes. Zhang et al. created triple conducting cathodes through self-assembly of $PrBaCo_{1.92}Zr_{0.08}O_{5+\delta}$ nanocomposites driven by

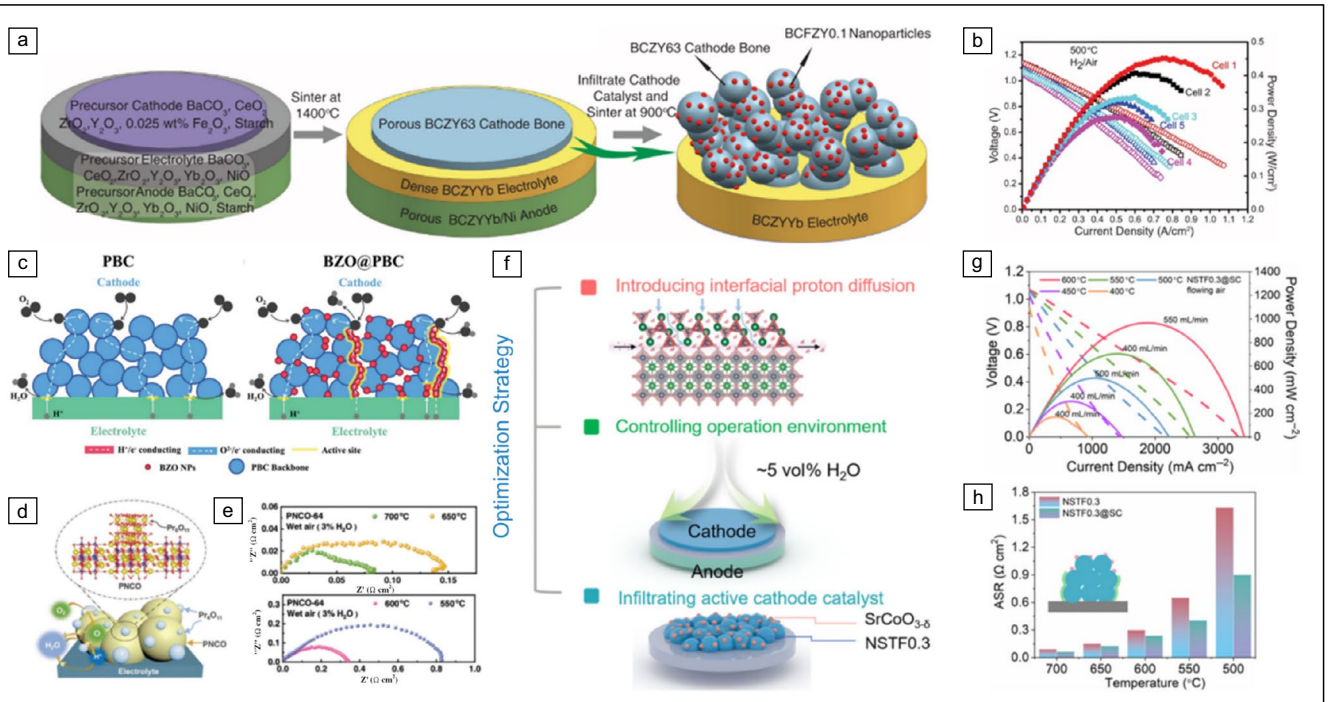

Figure 5. (a) Schematic illustration of the fabrication and structure of protonic ceramic fuel cell PCFC button cell with a composite cathode solid-state reactive sintering approach.[103] (b) *I–V* and power density of cells 1 to 5 under H_2/air at 500°C.[103] (c) Schematic illustration of surface self-assembly BZO-based NPs anchored on PBC substrate.[104] (d) Schematic illustration of the hybrid material PNCO-64 on the electrolyte supported symmetrical cell. (e) Electrical impediance spectra curves of symmetrical cells with the PNCO-64 cathodes.[105] (f) The optimization strategies for the NSTF0.3 cathode. (g) The *I–V* and power density curves of the single cell with NSTF0.3@SC. (h) The comparison of the polarization resistance of NSTF0.3 and NSTF0.3@SC symmetrical cells under the 5 vol% H_2O.[106] ASR, area specific resistance, NPs, nanoparticles.

surface protonation.[104] Under an oxidizing atmosphere, Ba/Zr cations spontaneously dissolve and form a proton-conductive phase $BaZrO_3$ (BZO) (Figure 5c). Surface reconstruction of heterogeneous structures improves structural stability, reduces thermal expansion, and accelerates oxygen reduction catalytic activity of this nanocomposite cathode. Recently, Xia et al. reported the development of a Co-doped RP perovskite ($Pr_2Ni_{0.6}Co_{0.4}O_{4-\delta}$), which self-configures into a composite of $Pr_4Ni_{1.8}Co_{1.2}O_{10-\delta}$ (PNCO, 89.57 wt%) and Pr_6O_{11} (10.43 wt%) (Figure 5d),[105] yielding improved activity with an area specific resistance (ASR) of 0.33 Ω cm^2 at 600°C after wet air treatment (Figure 5e). Similarly, a self-assembled composite cathode consisting of a $Na_ySr_zTi_uFe_{1-u}O_{3-\delta}$ (NSTF) active main phase and nanoscale β-$NaFeO_2$ (NF) structural domains to provide proton affinity was developed.[106] The cell with the composite cathode (NSTF0.3@SC) generated a PPD of 966 mW cm^2 at 600°C (Figure 5f–h) with enhanced ORR activity.

Fuel cells that operate at 200–400°C

Reducing the operation temperature to the range of 200–400°C can bring several benefits, including lower stack and system costs as well as the potential to utilize elastic polymer sealants. The 200–400°C range can be reached either by increasing the temperature of PEMFC-based devices or by further decreasing the temperature of SOFC/PCFC-based devices. We first begin with a discussion of increased-temperature PEMFCs.

During the past two decades, numerous efforts have been devoted to the development of effective and stable proton exchange materials for high-temperature (HT)-PEMFC. Currently, the state-of-the-art HT-PEMFCs utilize a series of phosphoric acid-doped polybenzimidazole (PA/PBI) polymers as the electrolyte, demonstrating promising power output and stability at 160−180°C. As opposed to the "vehicle" mechanism that transfers protons along with H_2O molecules in Nafion-based PEMFCs, the hydrogen-bond network composed between doped PA and the basic polymer skeleton facilitates proton migration in anhydrous conditions.[106] However, proton conductivity is primarily determined by the PA amount in the membranes, varying in the range of 50–240 mS cm^{-1} when the PA doping level is increased from 6 to 30 molecules per PBI polymer repeat unit.[107] Nevertheless, the cell performance drops quickly (e.g., by 50%) after just 35 h at a working temperature of 240°C due to uncontrollable acid loss associated with PA evaporation and dehydration at high temperatures.[108,109]

Recently, strategies have been developed to alleviate the acid loss at temperatures exceeding 200°C. One promising method is to fabricate composite membranes by doping hygroscopic fillers, such as clay and SiO_2, to bond more PA molecules in PA/PBI membranes.[110,111] As shown in **Figure 6**, some inorganic fillers undergo *in situ* transformation into proton-conducting metal pyrophosphates (MP_2O_7) in composite membranes during cell operation, exhibiting superior proton conductivity of 51.3 mS cm^{-1} at 250°C, with long-term stability over 50 h.[111] Note that the interior MP_2O_7 core plays a negligible role in proton transfer as no structural protons are incorporated in the lattice below 600°C; only the outer gel-like layer participates in the proton transfer.[110] Compared with simply mixing MP_2O_7 and PBI to synthesize MP_2O_7/PA/PBI composite membranes, the *in situ* formed membranes show better performance due to the homogenous distribution of MP_2O_7 fillers and the development of the outer proton-conducting layer on particle surfaces.[112] Among several fillers, SnO_2 presents a suitable reaction temperature around 250°C, which inhibits undesirable crystal growth and aggregation within the membrane, minimizing crack formation and alleviating deterioration of the mechanical properties.[111]

Considering that the acid loss at high temperatures is inevitable, the long-term stability of PA/PBI-based HT-PEMFCs remains concerning. This issue could be ultimately solved by the substitution of solid acids. A robust solid acid, $CsHSO_4$, was found to be a promising electrolytic substance for fuel cells operating at 100–300°C.[113] Typically, the performance of solid acid fuel cells (SAFCs) is influenced by three key factors: the thickness of the solid acid electrolyte, fuel humidification, and catalyst loading at the porous electrodes. CsH_2PO_4 and $CsHSO_4$ have emerged as archetypical SAFC electrolytes, exhibiting reasonably high proton conductivities of 2.2×10^{-2} S cm^{-1} at 240°C and 4×10^{-2} S cm^{-1} at 200°C, respectively.[114,115] Beyond utilizing a larger cation such as Rb and Cs to stabilize the solid acid, various elements (S, Se, P, and As) have been employed to tailor their super-protonic conductivity over a wider temperature range.[116,117] However, these electrolytes face critical challenges of poor mechanical and thermal stability, which can be partially mitigated by mixing oxide materials such as SiO_2, heteropoly acids, and ammonium polyphosphates.[118] In addition to these intrinsic durability issues, achieving a harmonious combination of low electrode impedance and low catalyst loading also remains a significant challenge. A prevailing strategy to enhance electrode performance in SAFCs involves nanostructuring each electrode to amplify the electrochemically active three-phase boundary density. Although Pt nanoparticles possess exceedingly high specific surface areas, the inherent tendency of Pt nanoparticles to aggregate during fuel-cell operation poses a threat to electrode performance.[119,120] Recently, several approaches by constructing supporting layers of graphitized nanoparticles, graphene flakes, and carbon nanotubes have been used to address the detrimental problem of catalyst aggregation. Additionally, methods such as impregnation, atomic layer deposition,[121] and metal–organic chemical vapor deposition[122] have been explored to load Pt nanoparticles onto support materials. Prospective endeavors in research should persist in investigating solid acids and electrode catalysts to further optimize performance and enhance SAFC durability. Key research directions should encompass the reduction of solid acid electrolyte thickness and the enhancement of supported catalyst stability.

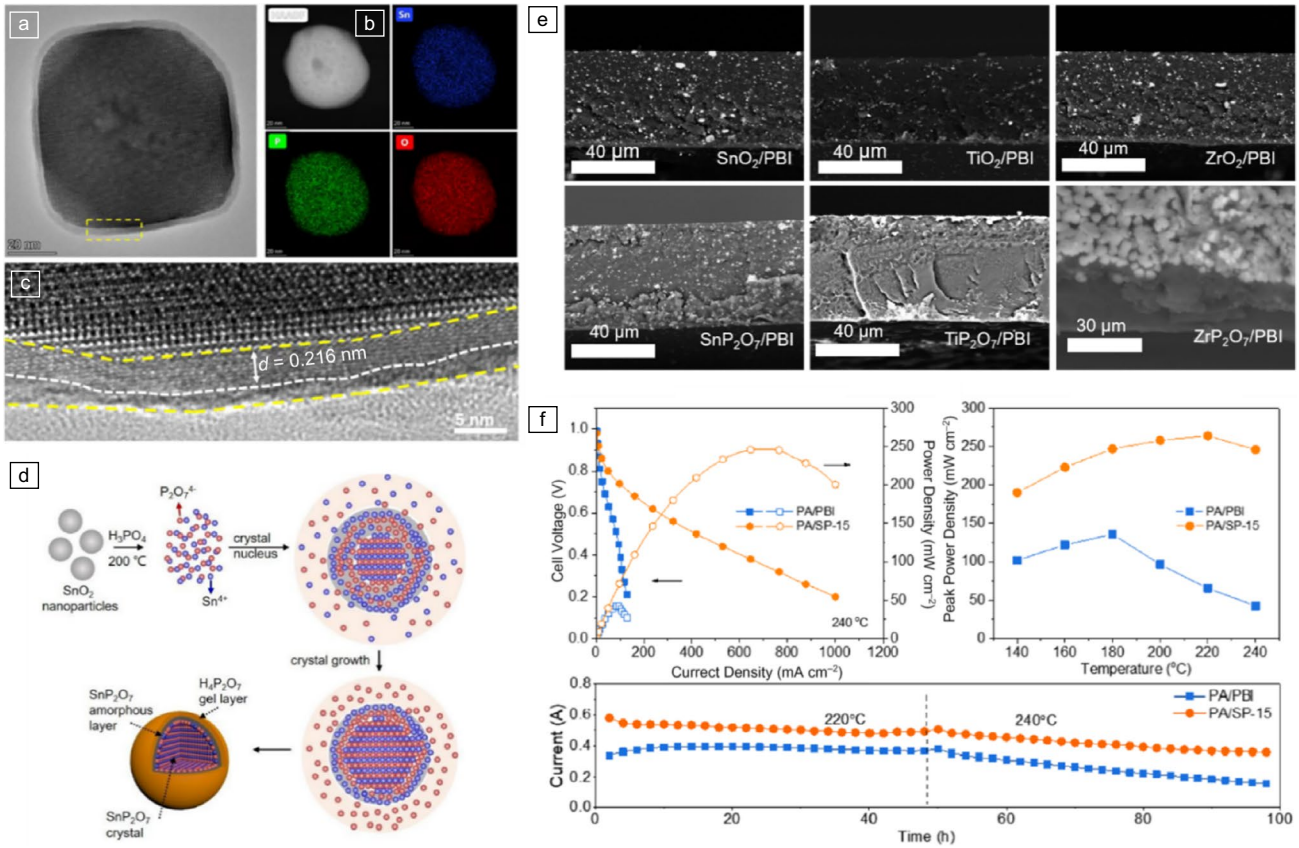

Figure 6. (a–c) Transmission electron microscopy and corresponding energy-dispersive spectroscopy mappings of Sn, O, and P elements of the core–shell SnP_2O_7. (d) Schematic illustration of growth of core–shell SnP_2O_7 between SnO_2 nanoparticles and PA at high temperatures. (e) Cross-section scanning transmission electron images of *in situ* formed MP_2O_7/PBI composite membranes with different inorganic nanofillers, showing the negative effect of the excessive aggregation and growth of MP_2O_7 in a PBI matrix. (f) Comparison of electrochemical performances regarding to *I–V* curves, conductivity, and stability in high-temperature (HT)-PEMFC single cell based on PA/PBI and *in situ* formed SnP_2O_7/PA/PBI membranes at different temperatures.[110,111]

Although, in principle, nonprecious metal catalysts could be applied at 200–400°C, the acidic nature of the electrolyte poses challenges in terms of both chemical stability and activity. As a result, Pt/C-based electrocatalysts are still necessary in both the anode and cathode. Theoretically, protons have much higher mobility than oxygen ions, which allows the operation of PCFCs at temperatures lower than 400°C. However, the actual electrolyte conductivity obtained in PCFC devices is still significantly lower than the expected value due to the poor sinterability and unfavorable interfacial contact resistance.[123] Very recently, as shown in **Figure 7**, Duan reported a new type of PCFC with an ultrathin BZCYYb electrolyte (approximately 3 μm), which successfully achieved a power density of ~200 mW cm^{-2} at 350°C in H_2-air.[124] The further development of PCFCs for operation at 200–400°C requires innovation in both electrolyte and electrode materials, as well as cell fabrication techniques.

Conclusion and perspectives

Fuel cells will likely play a significant role in the future carbon-neutral society. After more than a century of research, major progress in scientific understanding, materials innovation, and technological development has occurred. However, to realize widespread application, significant reduction in costs and improvements in cell durability are still needed, necessitating further innovations in electrode and electrolyte materials.

PEMFCs and SOFCs will continue to be the main focus due to their technical maturity and inherent advantages. To reduce PEMFC costs, the development of PGM-free electrocatalysts and further increases in cell operating temperature toward, or above 100°C are particularly promising research directions. To increase cell performance, further reductions in ohmic resistance through the development of thinner membranes as well as new electrolyte materials with higher conductivity are required. However, further

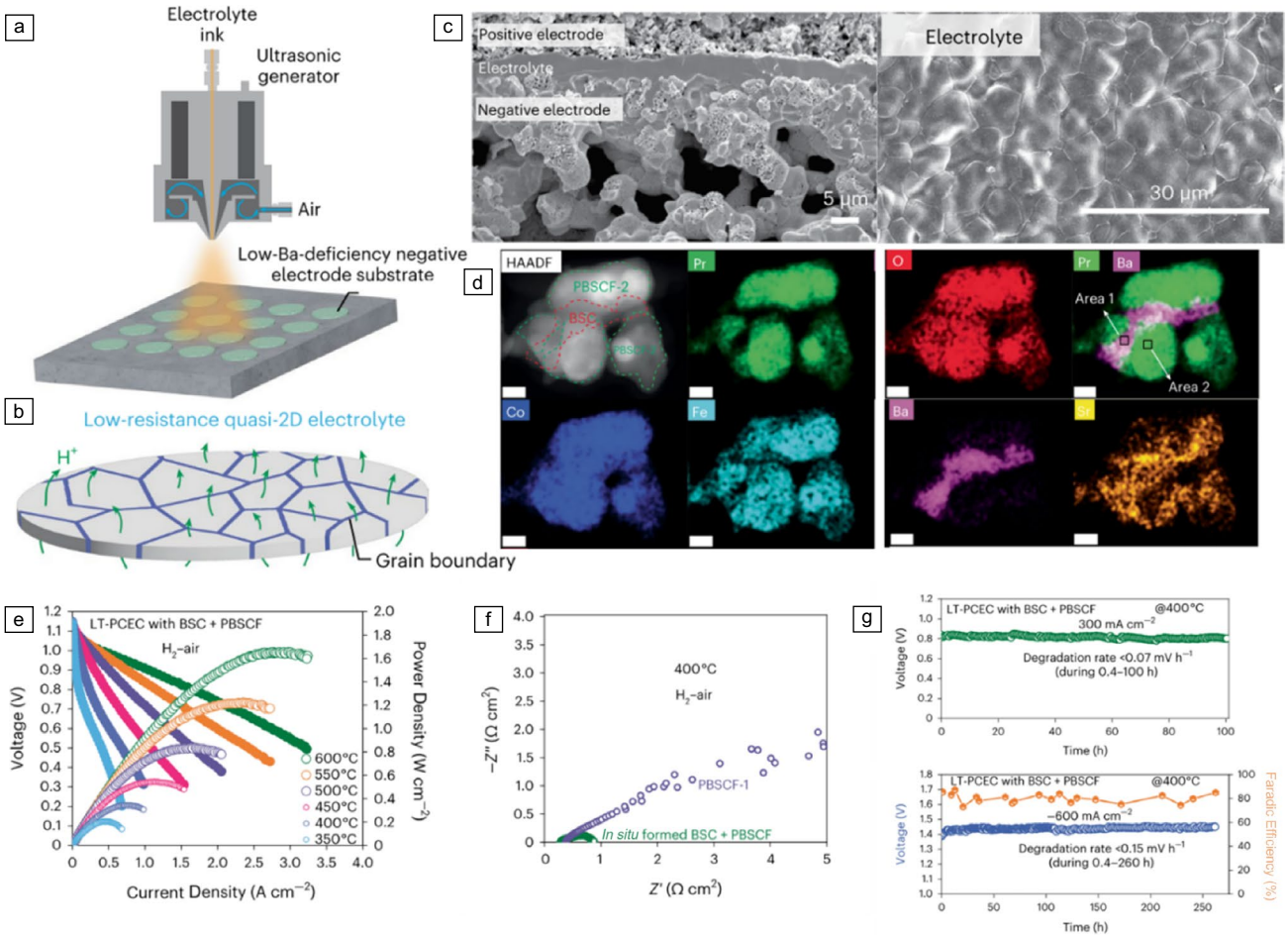

Figure 7. The schematic illustration of (a) the ultrathin (~3 μm) and dense electrolyte fabrication via spray-coating method, (b) the quasi-2D electrolyte. (c) Cross-section and surface scanning electron microscopy images of PCFC single cell, exhibiting ultrathin and dense BZCYYb electrolyte. (d) High-angle annular dark-field (HAADF) image and corresponding energy-dispersive spectroscopy mapping images of BSC/PBSCF composite materials as the PCFC cathode. (e) *I–V* curves of PCFC cell consist of BZCYYb electrolyte and BSC/PBSCF cathode at various operation temperatures. (f) Electrical impedance spectra of a specific cell tested under open-circuit voltage conditions at 400°C. (g) Stability testing of the single cell on H_2 air at 400°C in both fuel-cell and electrolysis modes.[123]

thickness reductions could be limited by membrane strength and reactant crossover issues. Here, polymer-enhanced composite membrane designs could help.[125] As compared to the anodic hydrogen oxidation reaction, ORR at the cathode is kinetically more difficult, in particular in acidic conditions.[126] By using an AEM electrolyte, the cathodic reaction kinetics are enhanced due to the basic environment, enabling the use of nonprecious metal catalysts even at room temperature.[127,128] The high cost and poor stability of available AEMs, however, is the main limit at the current stage. Although many nonprecious metals catalysts show favorable activity in alkaline solution,[59] their applicability in real AEMFCs is still limited due to their poor electronic conductivity. One intriguing application of PEMFCs/AEMFCs is as a portable power source using methanol as fuel.[129] In principle, DMFCs offer much higher energy density than the state-of-the-art lithium-ion batteries; however, due to the methanol crossover issue, very diluted methanol solution (1 M) is used, resulting in low energy efficiency, low energy density, and low power density.[130] The development of novel electrolyte membranes that can suppress methanol crossover will greatly facilitate practical DMFC application. Recently, it was reported that boron nitride (BN) and graphene show 100% proton diffusion selectivity with proton conductivity as high as 1 S cm^{-2} even at room temperature,[131,132] suggesting great potential for DMFC application. One big challenge is that both BN and graphene easily agglomerate in layers, resulting in substantially reduced apparent conductivity. Fabricating thin-film BN or graphene membranes that can avoid this issue while maintaining perfect gas tightness and sufficient mechanical strength is key to realize their practical use in fuel cells.

For SOFCs, reducing operation temperature to <600°C can greatly accelerate commercial application. In addition to improvements in cell fabrication, innovations in cell materials are needed. Considering the much higher mobility of protons versus oxygen ions, PCFCs are in principle more promising than conventional oxygen ion-based SOFCs. However, until now, PCFC cell performance has lagged that of conventional SOFCs. For reasons that are still poorly understood, the conductivity of protonic electrolytes in real cells is still much lower than it should be based on measurements of bulk materials.

Perovskite oxides by themselves do not natively contain protons, which are introduced externally through the hydration of oxygen vacancies, thus the conductivity is closely related to the hydration capability and oxygen vacancy concentration of the electrolyte. However, not all oxygen vacancies in the electrolyte membrane can be hydrated, and the remaining vacancies could act as impediments to proton diffusion. The consideration of alternative mechanisms for protonation could enable new electrolytes with higher conductivity at reduced temperatures. Intensive further study is required to confirm this observation. It is well known that protons can diffuse through both grain interiors and along grain boundaries. Some reports demonstrate that grain-boundary conduction could play a crucial role at lower temperatures.[133] Thus, the development of new electrolytes with facile grain-boundary conduction is also an interesting direction that requires more attention.

In PCFCs, water is formed at the cathode, and the competition between water and oxygen adsorption could lead to lower cathodic performance as compared to conventional SOFCs based on oxygen ion-conducting electrolytes. Thus, the cathode needs particular attention in PCFCs. Although there are many reported electrode materials, cobalt-based perovskite-type cathode materials generally demonstrate superior ORR activity, but durability is still concerning due to large coefficients of thermal expansion, poor chemical stability, low electronic conductivity, and potential deleterious reaction with common electrolytes.

In PCFCs, cathodes with oxygen ion, proton, and electronic "triple conductivity" are preferred to maximize the reaction kinetics. Recently, it was found that some single perovskites such as BCFZY demonstrate suitable triple conductivity at intermediate temperature.[134,135] Further, the formation of nanocomposites can enhance triple conductivity, a route worth further exploitation and development. Although fuel cells operating at 250−400°C bring many benefits, there are very few successful cases, mainly due to the lack of electrolyte materials and cathode materials that show sufficiently high conductivity or activity. PCFCs can potentially operate in this temperature range. However, further increase in proton conductivity and ORR activity is needed. The newly hydrogenation route for proton formation and/or exploitation of grain-boundary conduction mechanisms provide excellent opportunities for further study.

Author contributions

All authors drafted and critically revised the manuscript.

Funding

Open Access funding enabled and organized by CAUL and its Member Institutions. This work was supported by the Australian Research Council via Discovery Projects (Grant Nos. DP200103315, DP200103332, and DP230100685) and Industrial Transformation Research Hubs (IH220100012).

Data availability

No data for this perspective.

Conflict of interest

On behalf of all authors, the corresponding author states that there is no competing interest.

Open Access

References

1. T.M. Gür, *Prog. Energy Combust. Sci.* **89**, 100965 (2022)
2. W.R. Grove, *Philos. Mag.* **14**(89), 127 (1839)
3. L. Carrette, K.A. Friedrich, U. Stimming, *ChemPhysChem* **1**(4), 162 (2000)
4. E. Antolini, *Appl. Catal. B* **88**(1–2), 1 (2009)
5. S. Wang, S.P. Jiang, *Nat. Sci. Rev.* **4**(2), 163 (2017)
6. A. Qi, B. Peppley, K. Karan, *Fuel Process. Technol.* **88**(1), 3 (2007)
7. P. Vinchhi, M. Khandla, K. Chaudhary, R. Pati, *Inorg. Chem. Commun.* **152**, 110724 (2023)
8. H. Yokokawa, N. Sakai, T. Horita, K. Yamaji, M.E. Brito, *MRS Bull.* **30**(8), 591 (2005)
9. M.E. Scofield, H. Liu, S.S. Wong, *Chem. Soc. Rev.* **44**(16), 5836 (2015)
10. A. Parekh, *Front. Energy Res.* **10**, 956132 (2022)
11. J.F. Cao, Y.X. Ji, Z.P. Shao, *Energy Environ. Sci.* **15**(6), 2200 (2022)
12. A.V. Kasyanova, I.A. Zvonareva, N.A. Tarasova, L. Bi, D.A. Medvedev, Z.P. Shao, *Mater. Rep. Energy* **2**, 100158 (2022)
13. N. Mohammad, A.B. Mohamad, A.A.H. Kadhum, K.S. Loh, *J. Power Sources* **322**, 77 (2016)
14. A.L. Dicks, *Curr. Opin. Solid State Mater. Sci.* **8**(5), 379 (2004)
15. Y.X. Yang, P. Li, X.B. Zheng, W.P. Sun, S.X. Dou, T.Y. Ma, H.G. Pan, *Chem. Soc. Rev.* **51**, 9620 (2022)
16. K. Tanimoto, Y. Miyazaki, M. Yanagida, S. Tanase, T. Kojima, N. Ohtori, H. Okuyama, T. Kodama, *J. Power Sources* **39**(3), 285 (1992)
17. X.X. Wang, M.T. Swihart, G. Wu, *Nat. Catal.* **2**(7), 578 (2019)
18. S.M. Haile, *Acta Mater.* **51**(19), 5981 (2003)
19. B. Dalslet, P. Blennow, P.V. Hendriksen, N. Bonanos, D. Lybye, M. Mogensen, *J. Solid State Electrochem.* **10**, 547 (2006)
20. A.L. Ruth, K.T. Lee, M. Clites, E.D. Wachsman, *ECS Trans.* **64**(2), 135 (2014)
21. V.M. Zhukovskii, E.S. Buyanova, Y.V. Emel'yanova, M.V. Morozova, R.R. Shafigina, R.G. Zakharov, V.D. Zhuravlev, *Russ. J. Electrochem.* **45**, 512 (2009)
22. T. Matzke, M. Cappadonia, *Solid State Ionics* **86**, 659 (1996)

23. Y. Zhang, B. Chen, D. Guan, M. Xu, R. Ran, M. Ni, W. Zhou, R. O'Hayre, Z.P. Shao, *Nature* **591**(7849), 246 (2021)
24. V. Gil, J. Tartaj, C. Moure, *Ceram. Int.* **35**(2), 839 (2009)
25. W. Wang, D. Medvedev, Z.P. Shao, *Adv. Funct. Mater.* **28**(48), 1802592 (2018)
26. T. Wei, P. Singh, Y. Gong, J.B. Goodenough, Y.H. Huang, K. Huang, *Energy Environ. Sci.* **7**(5), 1680 (2014)
27. J.D. Fehribach, R. O'Hayre, *SIAM J. Appl. Math.* **70**(2), 510 (2009)
28. M. Wang, C. Su, Z.H. Zhu, H. Wang, L. Ge, *Compos. B Eng.* **238**, 109881 (2022)
29. S. Choi, T.C. Davenport, S.M. Haile, *Energy Environ. Sci.* **12**(1), 206 (2019)
30. T. Tsai, S.A. Barnett, *Solid State Ionics* **93**(3–4), 207 (1997)
31. Y. Zhang, G. Yang, G. Chen, R. Ran, W. Zhou, Z.P. Shao, *ACS Appl. Mater. Interfaces* **8**(5), 3003 (2016)
32. B. Gu, J. Sunarso, Y. Zhang, Y. Song, G. Yang, W. Zhou, Z.P. Shao, *J. Power Sources* **405**, 124 (2018)
33. J. Li, J. Hou, Y. Lu, Q. Wang, X. Xi, Y. Fan, X.-Z. Fu, J.-L. Luo, *J. Power Sources* **453**, 227909 (2020)
34. R. Ren, Z. Wang, C. Xu, W. Sun, J. Qiao, D.W. Rooneyc, K. Sun, *J. Mater. Chem. A* **7**, 18365 (2019)
35. D. Chen, G. Yang, Z.P. Shao, F. Ciucci, *Electrochem. Commun.* **35**, 131 (2013)
36. J.M. Ralph, C. Rossignol, R. Kumar, *J. Electrochem. Soc.* **150**(11), A1518 (2003)
37. A.L. Dicks, *J. Power Sources* **156**(2), 128 (2006)
38. D. Khalafallah, M. Zhi, Z. Hong, *ChemCatChem* **13**(1), 81 (2021)
39. W. Wang, C. Su, Y. Wu, R. Ran, Z.P. Shao, *Chem. Rev.* **113**(10), 8104 (2013)
40. M. Gong, X. Liu, J. Trembly, C. Johnson, *J. Power Sources* **168**(2), 289 (2007)
41. M. Vinothkannan, S. Ramakrishnan, A.R. Kim, H.K. Lee, D.J. Yoo, *ACS Appl. Mater. Interfaces* **12**, 5704 (2020)
42. H. Oh, B. Son, S. Shanmugam, *ACS Appl. Mater. Interfaces* **15**, 28093 (2023)
43. H. You, M. Vinothkannan, S. Shanmugam, *Mater. Today Chem.* **32**, 101634 (2023)
44. D. Taechaboonsermsak, C. Prapainainar, P. Kongkachuichay, M.P. Page, R.H. Naji, Z. Ji, J. Chen, Z. Guo, S.M. Holmes, P. Prapainainar, *Int. J. Hydrogen Energy* **52** (Pt. C), 1093 (2023). https://doi.org/10.1016/j.ijhydene.2023.09.069
45. C. Panawong, S. Tasarin, K. Phonlakan, J. Sumranjit, P. Saejueng, S. Budsombat, *Polymer* **244**, 124666 (2022)
46. Z. Meng, Y. Zou, N. Li, B. Wang, X. Fu, R. Zhang, S. Hu, X. Bao, X. Li, F. Zhao, Q. Liu, *ACS Appl. Energy Mater.* **6**, 1771 (2023)
47. G.G. Gagliardi, A. El-Kharouf, D. Borello, *Fuel* **345**, 128252 (2023)
48. J. Escorihuela, R. Narducci, V. Compañ, F. Costantino, *Adv. Mater. Interfaces* **6**, 1801146 (2019)
49. Y. Kang, J. Wang, Y. Wei, Y. Wu, D. Xia, L. Gan, *Nano Res.* **15**, 6148 (2022)
50. E.A. Lotf, M.V. Jacob, H. Ghassemi, M. Zakeri, M.M. Nasef, Y. Abdolahi, A. Abbasi, A. Ahmad, *Sci. Rep.* **11**, 3764 (2021)
51. L. Wang, M. Bellini, H.A. Miller, J.R. Varcoe, *J. Mater. Chem. A* **6**, 15404 (2018)
52. C.G. Arges, L. Zhang, *ACS Adv. Energy Mater.* **1**, 2991 (2018)
53. H. Chen, R. Tao, K.T. Bang, M. Shao, Y. Kim, *Adv. Energy Mater.* **12**, 2200934 (2022)
54. K. Yassin, I.G. Rasin, S.W. Cohen, C.E. Diesendruck, S. Brandon, D.R. Dekel, *J. Power Sources Adv.* **11**, 100066 (2021)
55. J.C. Douglin, J.R. Varcoe, D.R. Dekel, *J. Power Sources Adv.* **5**, 100023 (2020)
56. M.M. Hossen, M.S. Hasan, M.R.I. Sardar, J.B. Haider, Mottakin, K. Tammeveski, P. Atanassov, *Appl. Catal. B* **325**, 121733 (2023)
57. J. Tang, C. Su, Y. Zhong, Z.P. Shao, *J. Mater. Chem. A* **9**, 3151 (2021)
58. H. Adabi, A. Shakouri, N.U. Hassan, J.R. Varcoe, B. Zulevi, A. Serov, J.R. Regalbuto, W.E. Mustain, *Nat. Energy* **6**, 834 (2021)
59. X. Peng, T.J. Omasta, E. Magliocca, L. Wang, J.R. Varcoe, W.E. Mustain, *Angew. Chem. Int. Ed.* **58**(4), 1046 (2019)
60. D.R. Dekel, *Curr. Opin. Electrochem.* **12**, 182 (2018)
61. J. Durst, A. Siebel, C. Simon, F. Hasché, J. Herranz, H.A. Gasteiger, *Energy Environ. Sci.* **7**, 2255 (2014)
62. X. Yang, A.J.F. Carrión, X. Kuang, *Chem. Rev.* **123**, 9356 (2023)
63. D. Kim, I. Jeong, K.J. Kim, K.T. Bae, D. Kim, J. Koo, H. Yu, K.T. Lee, *J. Korean Ceram. Soc.* **59**, 131 (2022)
64. A. Chroneos, B. Yildiz, A. Tarancón, D. Parfitt, J.A. Kilner, *Energy Environ. Sci.* **4**, 2774 (2011)
65. N. Mahato, A. Banerjee, A. Gupta, S. Omar, K. Balani, *Prog. Mater. Sci.* **72**, 141 (2015)
66. J.W. Fergus, *J. Power Sources* **162**, 30 (2006)
67. N.Q. Minh, *J. Am. Ceram. Soc.* **76**, 563 (2005)
68. V. Kharton, F. Marques, A. Atkinson, *Solid State Ionics* **174**, 135 (2004)
69. L. Adijanto, R. Küngas, F. Bidrawn, R.J. Gorte, J.M. Vohs, *J. Power Sources* **196**, 5797 (2011)
70. B.H. Yun, C.W. Lee, I. Jeong, K.T. Lee, *Chem. Mater.* **29**, 10289 (2017)
71. M. Verkerk, A. Burggraaf, *J. Electrochem. Soc.* **128**, 75 (1981)
72. R. Chen, C.X. Li, C.J. Li, *J. Therm. Spray Technol.* **31**, 297 (2022)
73. E.D. Wachsman, K.T. Lee, *Science* **334**, 935 (2011)
74. T.N. Lin, M.C. Lee, R.J. Yang, J.C. Chang, W.X. Kao, L.S. Lee, *Mater. Lett.* **81**, 185 (2012)
75. K.N. Kim, J. Moon, J.W. Son, J. Kim, H.W. Lee, J.H. Lee, B.K. Kim, *J. Korean Ceram. Soc.* **42**, 637 (2005)
76. N. Wang, C. Tang, L. Du, R. Zhu, L. Xing, Z. Song, B. Yuan, L. Zhao, Y. Aoki, S. Ye, *Adv. Energy Mater.* **12**, 2201882 (2022)
77. L. Zhang, W. Sun, C. Xu, R. Ren, X. Yang, J. Qiao, Z. Wang, K. Sun, *J. Mater. Chem. A* **8**, 14091 (2020)
78. Y. Gao, Y. Ling, X. Wang, F. Jin, D. Meng, Z. Lv, B. Wei, *Chem. Eng. J.* **479**, 147665 (2024)
79. Z. Zhuang, Y. Li, R. Yu, L. Xia, J. Yang, Z. Lang, J. Zhu, J. Huang, J. Wang, Y. Wang, L. Fan, J. Wu, Y. Zhao, D. Wang, Y. Li, *Nat. Catal.* **5**, 300 (2022)
80. Y. Chen, S. Yoo, W. Zhang, J.H. Kim, Y. Zhou, K. Pei, N. Kane, B. Zhao, R. Murphy, Y. Choi, M. Liu, *ACS Catal.* **9**(8), 7137 (2019)
81. N. Osada, H. Uchida, M. Watanabe, *J. Electrochem. Soc.* **153**, A816 (2006)
82. M. Yang, C. Yang, M. Liang, G. Yang, R. Ran, W. Zhou, Z.P. Shao, *Molecules* **27**(23), 8396 (2022)
83. C.H. Lim, K.T. Lee, *Ceram. Int.* **42**, 13715 (2016)
84. K. Xu, H. Zhang, W. Deng, Y. Liu, Y. Ding, Y. Zhou, M. Liu, Y. Chen, *Sci. Bull.* **68**, 2574 (2023)
85. M.A. Peña, J. Fierro, *Chem. Rev.* **101**, 1981 (2001)
86. M.L. Faro, S.C. Zignani, A.S. Aricò, *Materials* (Basel) **13**, 3231 (2020)
87. N. Yu, T. Liu, X. Chen, M. Miao, M. Ni, Y. Wang, *Sep. Purif. Technol.* **291**, 120890 (2022)
88. S. Somacescu, N. Cioatera, P. Osiceanu, C.J.M. Moreno, C. Ghica, F. Neaţu, M. Florea, *Appl. Catal. B* **241**, 393 (2019)
89. Y. Song, W. Wang, L. Ge, X. Xu, Z. Zhang, P.S.B. Julião, W. Zhou, Z.P. Shao, *Adv. Sci.* **4**, 1700337 (2017)
90. Y. Xiang, D. Zheng, X. Zhou, H. Cai, K. Wang, C. Xia, X. Wang, W. Dong, H. Wang, B. Wang, *J. Am. Ceram. Soc.* **105**, 4457 (2022)
91. H. Yu, I. Jeong, S. Jang, D. Kim, H.N. Im, C.-W. Lee, E.D. Wachsman, K.T. Lee, *Adv. Mater.* **36**(5), e2306205 (2023)
92. K.D. Kreuer, S. Adams, W. Munch, A. Fuchs, U. Klock, J. Maier, *Solid State Ionics* **145**, 295 (2001)
93. L. Yang, S. Wang, K. Blinn, M. Liu, Z. Liu, Z. Cheng, M. Liu, *Science* **326**, 126 (2009)
94. T. Kuroha, Y. Niina, M. Shudo, G. Sakai, N. Matsunaga, T. Goto, K. Yamauchi, Y. Mikami, Y. Okuyama, *J. Power Sources* **506**, 230134 (2021)
95. C. Duan, J. Huang, N. Sullivan, R. O'Hayre, *Appl. Phys. Rev.* **7**, 011314 (2020)
96. R. Guo, D. Li, R. Guan, D. Kong, Z. Cui, Z. Zhou, T. He, *ACS Sustain. Chem. Eng.* **10**, 5352 (2022)
97. J. Lyagaeva, N. Danilov, G. Vdovin, J. Bu, D. Medvedev, A. Demin, P. Tsiakaras, *J. Mater. Chem. A* **4**, 15390 (2016)
98. M. Liang, Y. Song, D. Liu, L. Xu, M. Xu, G. Yang, W. Wang, W. Zhou, R. Ran, Z.P. Shao, *Appl. Catal. B* **318**, 121868 (2022)
99. J.H. Kim, J. Hong, D.K. Lim, S. Ahn, J. Kim, J.K. Kim, D. Oh, S. Jeon, S.J. Song, W. Jung, *Energy Environ. Sci.* **15**, 1097 (2022)
100. C. Lu, R. Ren, Z. Zhu, G. Pan, G. Wang, C. Xu, J. Qiao, W. Sun, Q. Huang, H. Liang, Z. Wang, K. Sun, *Chem. Eng. J.* **472**, 144878 (2023)
101. R. Ren, X. Yu, Z. Wang, C. Xu, T. Song, W. Sun, J. Qiao, K. Sun, *Appl. Catal. B* **317**, 121759 (2022)
102. Z. Liu, D. Cheng, Y. Zhu, M. Liang, M. Yang, G. Yang, R. Ran, W. Wang, W. Zhou, Z.P. Shao, *Chem. Eng. J.* **450**, 137787 (2022)
103. C. Duan, J. Tong, M. Shang, S. Nikodemski, M. Sanders, S. Ricote, A. Almansoori, R. O'Hayre, *Science* **349**, 1321 (2015)
104. X. Zhang, R. Song, D. Huan, K. Zhu, X. Li, H. Han, C. Xia, R. Peng, Y. Lu, *Small* **18**(49), 2205190 (2022)
105. J. Xia, F. Zhu, F. He, K. Xu, Y. Choi, Y. Chen, *Adv. Energy Mater.* **13**, 2302964 (2023)
106. D. Aili, D. Henkensmeier, S. Martin, B. Singh, Y. Hu, J.O. Jensen, L.N. Cleemann, Q. Li, *Electrochem. Energy Rev.* **3**, 793 (2020)
107. S. Yu, H. Zhang, L. Xiao, E.W. Choe, B.C. Benicewicz, *Fuel Cells* (Weinheim) **9**(4), 318 (2009)
108. V. Atanasov, A.S. Lee, E.J. Park, S. Maurya, E.D. Baca, C. Fujimoto, M. Hibbs, I. Matanovic, J. Kerres, Y.S. Kim, *Nat. Mater.* **20**, 370 (2021)
109. T. Søndergaard, L.N. Cleemann, H. Becker, T. Steenberg, H.A. Hjuler, L. Seerup, Q. Li, J.O. Jensen, *J. Electrochem. Soc.* **165**, F3053 (2018)
110. X. Wang, C. Dong, W. Zhao, P. Gao, G. Hou, S. Chen, S. Lu, H. Wang, Y. Xiang, J. Zhang, *Electrochim. Acta* **475**, 143588 (2024)
111. Z. Wang, J. Zhang, S. Lu, Y. Xiang, Z.P. Shao, S.P. Jiang, *Adv. Sustain. Syst.* **7**(3), 2200432 (2023)
112. Y.C. Jin, M. Nishida, W. Kanematsu, T. Hibino, *J. Power Sources* **196**, 6042 (2011)
113. S.M. Haile, D.A. Boysen, C.R.I. Chisholm, R.B. Merle, *Nature* **410**, 910 (2001)
114. C. Yang, P. Costamagna, S. Srinivasan, J. Benziger, A.B. Bocarsly, *J. Power Sources* **103**, 1 (2001)
115. S.M. Haile, C.R.I. Chisholm, K. Sasaki, D.A. Boysen, T. Uda, *Faraday Discuss.* **134**, 17 (2007)
116. V.V. Martsinkevich, V.G. Ponomareva, *Solid State Ionics* **225**, 236 (2012)
117. S. Afroze, M.S. Reza, M. Somalu, A.K. Azad, *Eurasian J. Phys. Funct. Mater.* **7**(1), 6 (2023)
118. V.G. Ponomareva, G.V. Lavrova, *Solid State Ionics* **145**, 197 (2001)
119. F.P. Lohmann-Richters, B. Abel, Á. Varga, *J. Mater. Chem. A* **6**, 2700 (2018)
120. F.P. Lohmann, P.S.C. Schulze, M. Wagner, O. Naumov, A. Lotnyk, B. Abel, Á. Varga, *J. Mater. Chem. A* **5**, 15021 (2017)

121. C. Liu, C. Wang, C. Kei, Y.C. Hsueh, T. Perng, *Small* **5**, 1535 (2009)
122. J. Klett, A. Eva, F. Heinz, B. Kaiser, W. Jaegermann, R. Schäfer, *ChemCatChem* **8**, 345 (2016)
123. S. Choi, C.J. Kucharczyk, Y. Liang, X. Zhang, I. Takeuchi, H.-I. Ji, S.M. Haile, *Nat. Energy* **3**(3), 202 (2018)
124. F. Liu, H. Deng, D. Diercks, P. Kumar, M.H.A. Jabbar, C. Gumeci, Y. Furuya, N. Dale, T. Oku, M. Usuda, P. Kazempoor, L. Fang, D. Chen, B. Liu, C. Duan, *Nat. Energy* **8**, 1145 (2023)
125. Y. Prykhodko, K. Fatyeyeva, L. Hespel, S. Marais, *Chem. Eng. J.* **409**, 127329 (2021)
126. Y. Hu, J.O. Jensen, C. Pan, L.N. Cleemann, I. Shypunov, Q. Li, *Appl. Catal. B* **234**, 357 (2018)
127. M.M. Hossen, M.S. Hasan, M.R.I. Sardar, J.B. Haider, Mottakin, K. Tammeveski, P. Atanassov, *Appl. Catal. B* **325**, 121733 (2023)
128. J. Lilloja, E. Kibena-Põldsepp, A. Sarapuu, M. Käärik, J. Kozlova, P. Paiste, A. Kikas, A. Treshchalov, J. Leis, A. Tamm, V. Kisand, S. Holdcroft, K. Tammeveski, *Appl. Catal. B* **306**, 121113 (2022)
129. S.K. Kamarudin, W.R.W. Daud, S.L. Ho, U.A. Hasran, *J. Power Sources* **163**, 743 (2007)
130. M. Ahmed, I. Dincer, *Int. J. Energy Res.* **35**, 1213 (2011)
131. L. Mogg, S. Zhang, G. Hao, K. Gopinadhan, D. Barry, B.L. Liu, H. Cheng, A.K. Geim, M. Lozada-Hidalgo, *Nat. Commun.* **10**, 4243 (2019)
132. S. Hu, M. Lozada-Hidalgo, F. Wang, A. Mishchenko, F. Schedin, R.R. Nair, E.W. Hill, D.W. Boukhvalov, M.I. Katsnelson, R.A.W. Dryfe, I.V. Grigorieva, H.A. Wu, A.K. Geim, *Nature* **516**, 227 (2014)
133. I.A. Starostina, G.N. Starostin, M.T. Akopian, G.K. Vdovin, D.A. Osinkin, B. Py, A. Maradesa, F. Ciucci, D.A. Medvedev, *Adv. Funct. Mater.* **34**(6), 2307316 (2023)
134. C. Zhou, D. Liu, M. Fei, X. Wang, R. Ran, M. Xu, W. Wang, W. Zhou, R. O'Hayre, Z.P. Shao, *J. Power Sources* **556**, 232403 (2023)
135. M. Liang, F. He, C. Zhou, Y. Chen, R. Ran, G. Yang, W. Zhou, Z.P. Shao, *Chem. Eng. J.* **420**, 127717 (2021) □

Zongping Shao is a John Curtin Distinguished Professor at Curtin University, Australia. He obtained his PhD degree from the Dalian Institute of Chemical Physics, China, in 2000. He has worked as a visiting scholar at Institut de Recherches sur la Catalyse, Centre National dse la Recherche Scientifique (CNRS), France, and as a postdoctoral researcher at the California Institute of Technology, from 2000 to 2005. His research interests include mixed conducting membranes for oxygen permeation, solid-oxide fuel cells, room-temperature electrocatalysts, batteries, supercapacitors, and solar cells. Shao can be reached by email at zongping.shao@curtin.edu.au.

Meng Ni joined The Hong Kong Polytechnic University in July 2009. He was appointed associate dean of the Faculty of Construction and Environment in 2021. He received his bachelor's degree in 2000 and master's degree in 2003 in aeroengine engineering. He received his PhD degree in mechanical engineering from The University of Hong Kong in 2007. His research interests include fuel cells, rechargeable metal–air batteries, electrochemical water-splitting, and electrochemical systems for low-grade waste heat utilization. Ni can be reached by email at meng.ni@polyu.edu.hk.